Letter

Robust stripes in the mixed-dimensional $t - J$ model

Henning Schlömer,[1,2] Annabelle Bohrdt,[3,4] Lode Pollet,[1,2] Ulrich Schollwöck,[1,2] and Fabian Grusdt[1,2]

[1]*Department of Physics and Arnold Sommerfeld Center for Theoretical Physics (ASC), Ludwig-Maximilians-Universität München, Theresienstr. 37, München D-80333, Germany*

[2]*Munich Center for Quantum Science and Technology (MCQST), Schellingstr. 4, München D-80799, Germany*

[3]*Department of Physics, Harvard University, Cambridge, Massachusetts 02138, USA*

[4]*ITAMP, Harvard-Smithsonian Center for Astrophysics, Cambridge, Massachusetts 02138, USA*

(Received 23 August 2022; accepted 17 February 2023; published 10 May 2023)

Microscopically understanding competing orders in strongly correlated systems is a key challenge in modern quantum many-body physics. For example, the origin of stripe order and its relation to pairing in the Fermi-Hubbard model remains one of the central questions, and may help to understand the origin of high-temperature superconductivity in cuprates. Here, we analyze stripe formation in the doped mixed-dimensional (mixD) variant of the $t - J$ model, where charge carriers are restricted to move only in one direction, whereas magnetic SU(2) interactions are two-dimensional. Using the density matrix renormalization group at finite temperature, we find a stable vertical stripe phase in the absence of pairing, featuring incommensurate magnetic order and long-range charge density wave profiles over a wide range of dopings. We find high critical temperatures on the order of the magnetic coupling $\sim J/2$, hence being within reach of current quantum simulators. Snapshots of the many-body state, accessible to quantum simulators, reveal hidden spin correlations in the mixD setting, whereby antiferromagnetic correlations are enhanced when considering purely the magnetic background. The proposed model can be viewed as realizing a parent Hamiltonian of the stripe phase, whose hidden spin correlations lead to the predicted resilience against quantum and thermal fluctuations.

DOI: 10.1103/PhysRevResearch.5.L022027

Introduction. The interplay of spin and motional degrees of freedom is at the heart of many strongly correlated quantum materials, leading to a plethora of interacting many-body phases. Microscopically understanding the competition between hole pairing and inhomogeneous stripe order in the paradigmatic Fermi-Hubbard (FH) model constitutes one of the central challenges in modern many-body physics, which may help to reveal the origin of high-temperature superconductivity [1–5]. In early experiments of cuprates and modern numerical studies of the FH model, the emergence of stripe order at low temperatures has been widely established [6–15]. However, it remains an open question whether pairing competes with stripes or if the two effects are different manifestations with a common origin [16–19].

Analog quantum simulation, e.g., via ultracold atoms, can help unveil the microscopic mechanisms underlying such strongly correlated phases [20–29]. In particular, recent advances allow for an implementation and experimental exploration of the FH model in ultracold atom setups [30–38]. However, studying stripe order with quantum simulators remains an open challenge, partly due to low critical temperatures [39] and close degeneracies of different stripe fillings and paired states [40].

Here, we propose a parent Hamiltonian whose ground state forms a robust stripe phase over a wide range of dopings. The model assumes mixed dimensionality (mixD), whereby motional degrees of freedom are restricted to be one-dimensional (1D), but spin-superexchange interactions are two-dimensional (2D). As a result, a similar pairing mechanism as proposed recently in mixD bilayer antiferromagnets (AFMs) [41] allows holes to form stable vertical stripes.

In this letter, we focus on general physical aspects of stripe order in the mixD setting. In particular, we analyze the order for various hole densities and map out the phase diagram. We predict high critical temperatures for stripe formation, rendering the stripe phase readily observable in ultracold atom experiments with optical lattices.

Our results shed new light on the long-standing question about the interplay of pairing and stripe formation. We find that the origin of stripes are hidden AFM correlations, making the stripe phase remarkably robust against thermal and quantum fluctuations. At the same time, intraleg pairing of two holes—the analog of a superconducting state—is strongly suppressed. The model is closely related to the celebrated 2D $t - J$ model, offering an adiabatic route to gain new insights into stripes and their related phases in the FH model.

We use finite temperature density matrix renormalization group (DMRG) methods via symmetry conserving purification schemes to predict thermal properties of the system with high accuracy.

Model. The proposed mixD $t - J$ model [42] describes mobile fermions whose motion is restricted to be along one

dimension, while their spin is coupled through 2D SU(2) invariant superexchange interactions. The Hamiltonian reads

$$\hat{\mathcal{H}} = -t \sum_{\sigma,\langle \mathbf{i},\mathbf{j}\rangle_x} \hat{\mathcal{P}}_{GW} (\hat{c}^\dagger_{\mathbf{i},\sigma} \hat{c}_{\mathbf{j},\sigma} + \text{H.c.}) \hat{\mathcal{P}}_{GW} + J \sum_{\langle \mathbf{i},\mathbf{j}\rangle} \left(\hat{\mathbf{S}}_\mathbf{i} \cdot \hat{\mathbf{S}}_\mathbf{j} - \frac{\hat{n}_\mathbf{i}\hat{n}_\mathbf{j}}{4} \right), \quad (1)$$

where $\hat{c}^{(\dagger)}_{\mathbf{i},\sigma}$, $\hat{n}_\mathbf{i}$, and $\hat{\mathbf{S}}_\mathbf{i}$ are fermionic annihilation (creation), particle density, and spin operators on site $\mathbf{i}$, respectively; $\langle \mathbf{i},\mathbf{j}\rangle_{(x)}$ denotes nearest-neighbor (NN) sites on the 2D square lattice (with subscript x indicating NN sites along the x direction only), and $\hat{\mathcal{P}}_{GW}$ is the Gutzwiller operator projecting out states with double occupancy. The mixD $t-J$ model Hamiltonian, Eq. (1), features a global SU(2) spin and individual U(1) particle conservation symmetries in each chain, $\ell = 1 \ldots L_y$.

The mixD setup in Eq. (1) can be realized by simulating the Fermi-Hubbard model in the large U/t limit with a strong onsite linear potential along y, i.e., $V_{\text{tilt}}(y) = \Delta y$ [43–45]. The potential gradient Δ effectively suppresses resonant tunneling along y, whereas virtual particle exchanges (and hence spin superexchange) remain intact – hence realizing the mixD $t-J$ setting, see Ref. [46] for a more detailed discussion.

Ground state properties. Using DMRG [47–51], we calculate ground state properties of the doped mixD $t-J$ model Eq. (1) on ladder geometries by explicitly implementing the U(1) particle conservation symmetry in each leg separately. The explicit use of tensors with the Hamiltonian's enhanced symmetry greatly decreases computational costs, whereby speedup factors of $\gtrsim$10 for bond dimensions $\chi \sim 10\,000$ are reached.

From now on, we use an equal number of holes in each leg, i.e., $N_\ell = N^h$ for all, $\ell = 1 \ldots L_y$, and choose $t/J = 3$. The color coded background in Fig. 1(a) shows spin-spin correlations $\langle \hat{S}^z_{\mathbf{i}_0} \hat{S}^z_\mathbf{j} \rangle$ with fixed reference site $\mathbf{i}_0$ in the center of the second leg for a system of size $L_x \times L_y = 40 \times 4$ with open (periodic) boundaries along x (y). Grey filled lines depict local hole densities $\langle \hat{n}^h_\mathbf{i} \rangle$ in each leg. In the ground state, we see clear indications for the formation of fully filled stripes, by observing (i) a periodic modulation of hole densities, and (ii) the appearance of AFM domain walls at positions of maximum hole density.

The latter is further underlined in the lower left panel of Fig. 1(a), where the spin-spin correlations are shown for the central $y = 2$ region. Correlations are observed to be incommensurate with the lattice, i.e., the total number of peaks in the spin-correlation function in each ladder leg – given by $N_p = 18$ in Fig. 1(a) – is incommensurate with the length of the system $L_x = 40$. This corresponds to a modulation of spin correlation with wavelength $\lambda = (1-n^h)^{-1}$, where $n^h = N^h/L_x$. Emerging incommensurate antiferromagnetic order is further revealed in the static spin structure factor along leg y:

$$\mathcal{S}_y(q_x) = \frac{1}{L_x} \sum_{x_1,x_2} \langle \hat{S}^z_{[x_1,y]} \hat{S}^z_{[x_2,y]} \rangle \exp[iq_x(x_1 - x_2)], \quad (2)$$

which features a double-peak structure at points $q_x^{\max} = \pi(1 \pm n^h)$, depicted in the lower right panel of Fig. 1(a). When increasing the doping level, incommensurate magnetic order

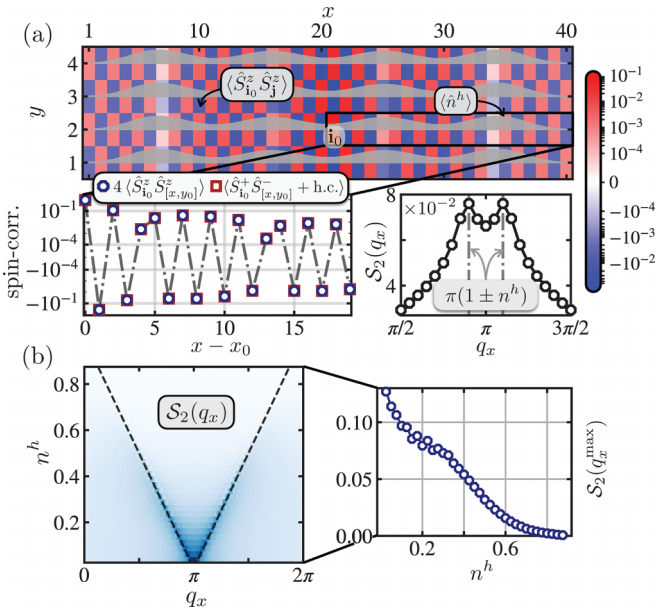

FIG. 1. Ground state properties. (a) Spin-spin correlations $\langle \hat{S}^z_{\mathbf{i}_0} \hat{S}^z_\mathbf{j} \rangle$ with reference site $\mathbf{i}_0 = [x_0 = 21, y_0 = 2]$ for a 40×4 system with $n^h = 0.1$. Boundaries are open (closed) in x (y) direction. Correlations are color coded using a symmetric logarithmic scale, with linear scaling between $-10^{-4} \ldots 10^{-4}$. Average hole densities $\langle \hat{n}^h_\mathbf{i} \rangle$ are shown in grey. Lower left panel: correlation functions $4\,\langle \hat{S}^z_{\mathbf{i}_0} \hat{S}^z_{[x,y_0]} \rangle$, $\langle \hat{S}^+_{\mathbf{i}_0} \hat{S}^-_{[x,y_0]} + \text{H.c.} \rangle$, which are indistinguishable on the scale of the plot. Dot-dashed grey lines connecting the data points underline the incommensurate peak structure of spin correlations. Lower right panel: static spin structure factor along $y = 2$, Eq. (2), with peaks located at $q_x = \pi(1 \pm n^h)$. (b) Left panel: Spin structure factor of the central leg as a function of doping n^h for a 40×3 system. A narrower system size is chosen to keep numerical costs reasonable. Open boundaries are taken to avoid magnetic frustration of the ladder. Right panel: Peak height $\mathcal{S}_2(q_x^{\max})$ at $q_x^{\max} = (1-n^h)\pi$ as a function of doping n^h.

and stripes persist, however with overall decreasing magnetic order due to the enhanced disturbance by the holes, cf. Fig. 1(b). Beyond $n^h \gtrsim 0.5$, no clear signs of stripe formation are visible anymore.

We note that charge-density wavelike correlations are also expected in purely 1D systems with open boundaries. The oscillation amplitudes of such Friedel oscillations away from the edges decay as r^{-K}, with K the Luttinger exponent [52]. In contrast, in the mixD setting the amplitude of the charge modulations quickly converges towards a constant plateau, i.e., they are present even deep in the bulk. We explicitly compare the density oscillations in long 1D and mixD systems in [46].

On cylinders of width $L_y = 4$, we evaluate the intraleg binding energy of two holes $E_b = [E(2) - E(0)] - 2[E(1) - E(0)]$, where $E(N^h)$ is the ground state energy of a mixD cylinder with N^h holes doped into a single ladder leg. We find almost vanishing binding energies of order $E_b/t \sim \mathcal{O}(10^{-3})$ in our finite-size simulations, strongly supporting the absence of hole-pairing in the mixD $t-J$ model. This is further underlined by features of connected hole-hole correlators,

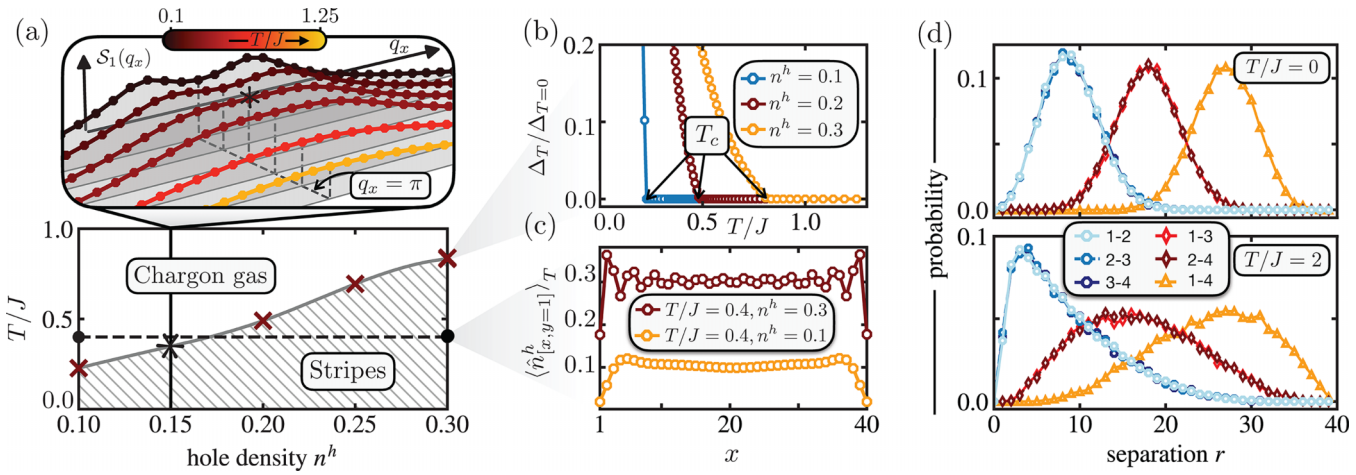

FIG. 2. Finite temperature properties. (a) Lower panel: Phase diagram of the mixD $t-J$ model for a 40×2 system (OBC). In the stripe phase, charge- and spin-density waves are present, whereas in the chargon gas phase holes can move freely and AFM spin correlations are short-range. We define the critical temperature $T_c(n^h)$ as the point where the double peak of the spin structure factor washes out into a single broad peak, illustrated for $n^h = 0.15$ in the upper panel of (a) and marked by an asterisk. Temperatures $T/J = 1.25, 0.83, 0.4, 0.35, 0.25, 0.1$ are shown, ranging from yellow to dark red upon lowering the temperature. (b) Peak split $\Delta_T/\Delta_{T=0}$, with $\Delta_T = S(q_x^{\max}) - S(\pi)$, as a function of temperature. (c) Hole density profiles $\langle \hat{n}^h_{[x,y=1]} \rangle_T$ for $n^h = 0.1, 0.3$ at constant temperature $T/J = 0.4$ [solid dots connected by dashed line in (a)]. In the stripe phase, clear charge oscillation signals in the hole density profile are visible, whereas in the chargon gas the profile is flat. (d) Full counting statistics of hole distances along a single ladder leg for $n^h = 0.1$ and $T/J = 0, 2$ (notation $i-j$ corresponds to the distance r between hole i and hole j along x). In the stripe phase (upper panel), the probability distributions are symmetric, whereas in the chargon gas (lower panel), hole-hole distance probability distributions acquire long tails. We use 20,000 snapshots of the (thermal) MPS.

revealing how at short distances, holes strongly repel each other, whereas binding in stripes is favored [46].

Finite temperature. In order to estimate critical temperatures for stripe formation, we use mixed-state purification and imaginary time evolution schemes while conserving the system's symmetries [46,53–55]. In particular, during the time evolution we conserve the particle number in each physical leg N_ℓ, $\ell = 1..L_y$, the total particle number in the auxiliary system $N^{\text{tot}}_{\text{aux.}}$, as well as the total spin $S^{z,\text{tot}}_{\text{phys.+aux.}}$ (the latter allowing for finite total magnetizations of the physical system at finite temperature). This results in a total of $L_y + 2$ symmetries employed by the finite temperature implementation.

Utilizing the enhanced symmetry, we are able to accurately evolve the system down to low temperatures, allowing us to evaluate convergence towards the ground state [46]. Due to the effective doubling of the width of the system after purification, we restrict the following discussion to systems with $L_y = 2$. Numerical results for wider systems are presented in [46]. For the time evolution schemes, we again use maximal bond dimensions $\chi \sim 10,000$.

Results for a 40×2 physical system with open boundary conditions (OBC) are shown in Fig. 2. Starting from high temperatures, we measure the static spin structure factor, localize its peak position $\pm q_x^{\max}$ and calculate the peak split parameter defined by $\Delta_T = \mathcal{S}_y(q_x^{\max}) - \mathcal{S}_y(\pi)$. The upper panel of Fig. 2(a) shows the structure factor for various temperatures. At high temperatures, correlations are short-range and in particular commensurate with the lattice, i.e., the structure factor is characterized by a broad peak around $q_x = \pi$ and $\Delta_{T>T_c}$ is strictly zero. Upon lowering the temperature to the critical value T_c, a finite split in the structure factor is observed, i.e., incommensurate magnetic features emerge. The transition point is marked by an asterisk in the upper panel of Fig. 2(a).

Figure 2(b) underlines the definition of the critical temperature, where the peak split becomes finite, i.e., $\Delta_{T<T_c} > 0$. The corresponding critical temperatures as a function of hole doping are plotted in the lower panel of Fig. 2(a), for hole densities ranging from $n^h = 0.1...0.3$. Note how critical temperatures are of the order of magnitude $\sim J/2$, rendering the stripe phase significantly more robust against thermal fluctuations in the mixD setting compared to its analog in 2D [39,40].

We illustrate the emergence of stripes further by showing the average hole density profile for two different doping levels while keeping the temperature constant, Fig. 2(c). For $T/J = 0.4$ and $n^h = 0.1$, the hole density forms a flat plateau, i.e., there is no charge order and holes are in a deconfined chargon gas phase (i.e., holes are not confined within stripes and move freely through the magnetic background) [56]. In contrast, clear charge oscillations are visible for $n^h = 0.3$, underlining how in the stripe phase both charge and spin density waves are present. By computing the charge structure factor, we have checked that charge order is present over the whole range of temperatures $T < T_c(n^h)$, in fact setting in at slightly higher temperatures than incommensurate magnetic order. This is characteristic for a crossover driven by the charges [2,57], as is the case for the chargon gas to stripe transition observed here.

Note that the Néel temperature of the SU(2) symmetric 2D Heisenberg model is strictly zero, however with a magnetic correlation length scaling as $\sim e^{T_0/T}$. Akin to the cold atom antiferromagnet realized in Ref. [29], we argue that stripe features—that is, the emergence of charge- and spin-density wave patterns—become visible on the length scale of the system size for temperatures below T_c. For sufficiently strong magnetic correlations, we expect that true long-range charge order (breaking the discrete translational symmetry of the

system) is stabilized at finite temperatures also in the thermodynamic limit $L_x, L_y \to \infty$.

Snapshots and hidden correlations. In quantum gas microscopy experiments, projective measurements are taken in the Fock basis of the many-body state. These snapshots contain a plethora of information about the system beyond averages and local observables, allowing for further insights into the quantum many-body wave function [58]. Using (thermal) matrix product states, we sample independent snapshots via the perfect sampling approach [59,60].

Figure 2(d) illustrates the stripe-chargon gas crossover by full counting statistics of hole-hole distances within a single ladder leg. In the stripe phase, probability distributions for hole-hole distances are symmetrically peaked around a maximal distance probability. On the other hand, in the chargon gas phase the discrete probability distributions develop long tails, i.e., mean and maximum are far separated from another. These kind of rare event distributions often govern the physics of the system [61], here indicating a phase of freely moving, deconfined holes through the magnetic background.

A further major advantage of the restricted hole motion is that we can uniquely define squeezed space [35,62], where holes are removed (i.e., "squeezed out") from each snapshot before measuring observables, cf. Fig. 3(a). Spatially separating occupied and unoccupied sites by squeezing allows to analyze the interplay between hole motion and magnetism in more detail, explicitly utilizing nonlocal information contained in snapshots of the many-body wave function.

Figure 3(b) shows the spin structure factor along $y = 1$ of a 40×2 mixD $t - J$ model in the ground state (i.e., in the stripe phase) in real (black circles) and squeezed (red squares) space after removing holes from the snapshots. When transforming ground state snapshots to squeezed space, hidden AFM correlations are revealed, i.e., the double peak structure turns into a sharp peak around $q_x = \pi$. Indeed, when comparing to the pure Heisenberg model [63] with $J = 1$, both structure factors agree on a quantitative level, showing how the holes confined within the stripes leave the underlying magnetic state in squeezed space almost undisturbed.

In the chargon gas phase, on the other hand, the movement of the holes distorts the magnetic background in a more notable manner. Black circles in Fig. 3(c) show $\mathcal{S}_1(q_x)$ evaluated via the thermal MPS at $T/J = 5/7 \approx 0.71$. When transforming snapshots to squeezed space, the initially broad peak around $q_x = \pi$ again becomes significantly sharper, showing how AFM correlations are reduced due to the holes' motion through the Mott insulator. Compared to the Heisenberg model with $J = 1$ at $T/J = 5/7 \approx 0.71$ [blue circles in Fig. 3(c)], the squeezed mixD system has shifted weight from AFM ($q_x = \pi$) to more FM ($q_x = 0, 2\pi$) correlations. Enhanced FM signals in squeezed space emerge due to the frustrating effect of hole motion on spins in squeezed space, which is analyzed and quantified in detail by some of us in Ref. [64].

Discussion. In this letter, we presented numerical DMRG results that demonstrate the formation of stable stripes in the $t - J$ model of mixed dimensionality. Above critical temperatures T_c on the order of J, we find commensurate, short-range antiferromagnetic correlations together with deconfined holes. Below the critical temperature, incommensurate order as well

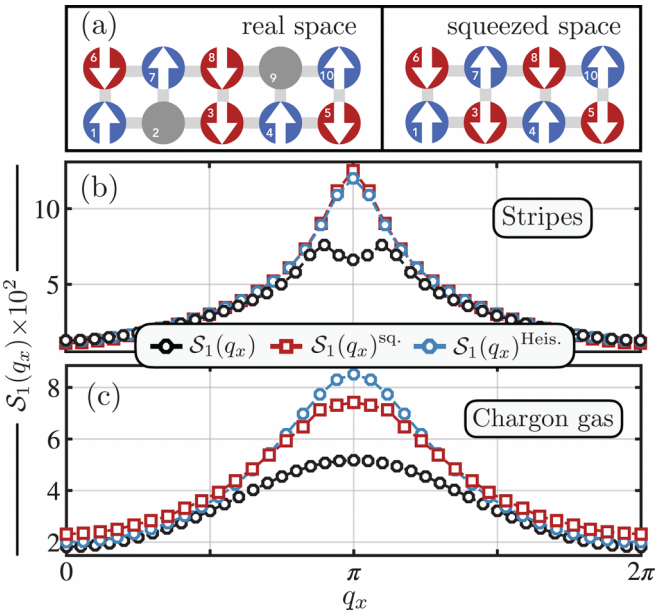

FIG. 3. (a) Illustration of squeezed space. Left panel: Snapshot of holes moving through a Néel background. Right panel: Upon squeezing out the holes, Néel order is restored in the magnetic background. (b) Spin structure factor $\mathcal{S}_1(q_x)$ for a mixD $t - J$ system in the striped ground state with $n^h = 0.1$, featuring a double-peak structure in real space (black circles). Squeezing snapshots reveals hidden AFM correlations (red squares), being in quantitative agreement with the $J = 1$ Heisenberg ground state (blue circles). (c) The same for the chargon gas phase at $T/J = 5/7 \approx 0.71$, $n^h = 0.15$. Upon squeezing, the peak around $q_x = \pi$ becomes considerably sharper. Compared to the pure Heisenberg model with $J = 1$ and $T/J = 5/7 \approx 0.71$ (light blue circles), the spin structure in the chargon gas phase has a shifted weight towards FM correlations. For both cases above, the mixD system is of size 40×2.

as charge density waves emerge on long length scales of the numerically accessible system size, i.e., stripes form in the system. Our work extends the strong pairing mechanism proposed in bilayer Hubbard models [41] and realized in mixD ultracold atom setups [37], to stabilize stripes at high temperatures.

Observations of strong AFM correlations in three dimensional (3D) realizations of the FH model [30] motivate the existence of resilient sheets of stripes in a possible generalization of the mixD $t - J$ model to 3D, where —in contrast to 2D —true long-range magnetic order appears also at finite temperature.

Recently, the mixD t-J_z model including solely Ising-type interactions has been analyzed [56]. There, an exact mapping revealed an emergent $\mathbb{Z}_2$ lattice gauge structure, which allowed to draw analogies with gauge theories and distinguish phases by emergent properties. The mixD t-J_z model has been shown to exhibit a rich phase diagram when restricted to a single gauge sector (i.e., a fixed AFM Néel background), including stripes, a deconfined chargon gas as well as a meson gas, where in the latter holes form pairs at low hole concentrations and temperatures slightly above T_c. It remains to be analyzed whether a confined phase of mesonic character exists

also in the mixD t-J model (including spin fluctuations as well as gauge mixing in comparison to [56]), and if any conclusive connections can be drawn in the context of $\mathbb{Z}_2$ lattice gauge theories.

Acknowledgments. We are thankful for valuable discussions with S. Paeckel, Z. Zhu, S. Mardazad, L. Rammelmüller, J. Dicke, F. Palm, M. Kebric, S. Haas, I. Bloch, T. Hilker, S. Hirthe, D. Bourgund, and P. Bojovic. This research was funded by the Deutsche Forschungsgemeinschaft (DFG, German Research Foundation) under Germany's Excellence Strategy—EXC-2111390814868, by the European Research Council (ERC) under the European Union's Horizon 2020 research and innovation programme (Grant Agreement No. 948141), by the FP7/ERC Consolidator Grant QSIMCORR, No. 771891, and by the NSF through a grant for the Institute for Theoretical Atomic, Molecular, and Optical Physics at Harvard University and the Smithsonian Astrophysical Observatory.

[1] A. S. Darmawan, Y. Nomura, Y. Yamaji, and M. Imada, Stripe and superconducting order competing in the Hubbard model on a square lattice studied by a combined variational Monte Carlo and tensor network method, Phys. Rev. B **98**, 205132 (2018).

[2] V. Emery, S. Kivelson, and J. Tranquada, Stripe phases in high-temperature superconductors, Proc. Natl. Acad. Sci. **96**, 8814 (1999).

[3] A. Himeda, T. Kato, and M. Ogata, Stripe States with Spatially Oscillating d-Wave Superconductivity in the Two-Dimensional $t-t'-J$ Model, Phys. Rev. Lett. **88**, 117001 (2002).

[4] A. Bianconi, D. Di Castro, G. Bianconi, A. Pifferi, N. L. Saini, F. C. Chou, D. C. Johnston, and M. Colapietro, Coexistence of stripes and superconductivity: Tc amplification in a superlattice of superconducting stripes, Physica C: Superconductivity **341-348**, 1719 (2000).

[5] J. M. Tranquada, Stripes and superconductivity in cuprates, Phys. B: Condens. Matter **407**, 1771 (2012).

[6] A. Georges, G. Kotliar, W. Krauth, and M. J. Rozenberg, Dynamical mean-field theory of strongly correlated fermion systems and the limit of infinite dimensions, Rev. Mod. Phys. **68**, 13 (1996).

[7] S. A. Kivelson, I. P. Bindloss, E. Fradkin, V. Oganesyan, J. M. Tranquada, A. Kapitulnik, and C. Howald, How to detect fluctuating stripes in the high-temperature superconductors, Rev. Mod. Phys. **75**, 1201 (2003).

[8] K. Machida, Magnetism in La_2CuO_4 based compounds, Physica C: Superconductivity **158**, 192 (1989).

[9] J. Zaanen and O. Gunnarsson, Charged magnetic domain lines and the magnetism of high-T_c oxides, Phys. Rev. B **40**, 7391 (1989).

[10] S. R. White and D. J. Scalapino, Density Matrix Renormalization Group Study of the Striped Phase in the 2d $t-J$ Model, Phys. Rev. Lett. **80**, 1272 (1998).

[11] S. R. White and D. J. Scalapino, Stripes on a 6-Leg Hubbard Ladder, Phys. Rev. Lett. **91**, 136403 (2003).

[12] G. Hager, G. Wellein, E. Jeckelmann, and H. Fehske, Stripe formation in doped Hubbard ladders, Phys. Rev. B **71**, 075108 (2005).

[13] G. Ehlers, S. R. White, and R. M. Noack, Hybrid-space density matrix renormalization group study of the doped two-dimensional hubbard model, Phys. Rev. B **95**, 125125 (2017).

[14] Y.-F. Jiang, J. Zaanen, T. P. Devereaux, and H.-C. Jiang, Ground state phase diagram of the doped hubbard model on the four-leg cylinder, Phys. Rev. Res. **2**, 033073 (2020).

[15] E. W. Huang, T. Liu, W. O. Wang, H.-C. Jiang, P. Mai, T. A. Maier, S. Johnston, B. Moritz, and T. P. Devereaux, Fluctuating intertwined stripes in the strange metal regime of the Hubbard model, Phys. Rev. B **107**, 085126 (2023).

[16] P. Corboz, T. M. Rice, and M. Troyer, Competing States in the t-j Model: Uniform d-Wave State Versus Stripe State, Phys. Rev. Lett. **113**, 046402 (2014).

[17] B. X. Zheng and G. K.-L. Chan, Ground-state phase diagram of the square lattice hubbard model from density matrix embedding theory, Phys. Rev. B **93**, 035126 (2016).

[18] M. Qin, Stripes versus superconductivity in the doped Hubbard model on the honeycomb lattice, Phys. Rev. B **105**, 035111 (2022).

[19] M. Qin, C.-M. Chung, H. Shi, E. Vitali, C. Hubig, U. Schollwöck, S. R. White, and S. Zhang (Simons Collaboration on the Many-Electron Problem), Absence of Superconductivity in the Pure Two-Dimensional Hubbard Model, Phys. Rev. X **10**, 031016 (2020).

[20] I. Bloch, J. Dalibard, and S. Nascimbène, Quantum simulations with ultracold quantum gases, Nat. Phys. **8**, 267 (2012).

[21] I. Bloch, J. Dalibard, and W. Zwerger, Many-body physics with ultracold gases, Rev. Mod. Phys. **80**, 885 (2008).

[22] C. Gross and I. Bloch, Quantum simulations with ultracold atoms in optical lattices, Science **357**, 995 (2017).

[23] F. Schäfer, T. Fukuhara, S. Sugawa, Y. Takasu, and Y. Takahashi, Tools for quantum simulation with ultracold atoms in optical lattices, Nat. Rev. Phys. **2**, 411 (2020).

[24] J. Koepsell, D. Bourgund, P. Sompet, S. Hirthe, A. Bohrdt, Y. Wang, F. Grusdt, E. Demler, G. Salomon, C. Gross, and I. Bloch, Microscopic evolution of doped Mott insulators from polaronic metal to Fermi liquid, Science **374**, 82 (2021).

[25] E. Zohar, J. I. Cirac, and B. Reznik, Quantum simulations of lattice gauge theories using ultracold atoms in optical lattices, Rep. Prog. Phys. **79**, 014401 (2016).

[26] L. W. Cheuk, M. A. Nichols, M. Okan, T. Gersdorf, V. V. Ramasesh, W. S. Bakr, T. Lompe, and M. W. Zwierlein, Quantum-Gas Microscope for Fermionic Atoms, Phys. Rev. Lett. **114**, 193001 (2015).

[27] A. Omran, M. Boll, T. A. Hilker, K. Kleinlein, G. Salomon, I. Bloch, and C. Gross, Microscopic Observation of Pauli Blocking in Degenerate Fermionic Lattice Gases, Phys. Rev. Lett. **115**, 263001 (2015).

[28] M. F. Parsons, F. Huber, A. Mazurenko, C. S. Chiu, W. Setiawan, K. Wooley-Brown, S. Blatt, and M. Greiner, Site-Resolved Imaging of Fermionic ^{6}Li in an Optical Lattice, Phys. Rev. Lett. **114**, 213002 (2015).

[29] A. Mazurenko, C. S. Chiu, G. Ji, M. F. Parsons, M. Kanász-Nagy, R. Schmidt, F. Grusdt, E. Demler, D. Greif, and M.

Greiner, A cold-atom Fermi-Hubbard antiferromagnet, Nature (London) **545**, 462 (2017).

[30] R. A. Hart, P. M. Duarte, T.-L. Yang, X. Liu, T. Paiva, E. Khatami, R. T. Scalettar, N. Trivedi, D. A. Huse, and R. G. Hulet, Observation of antiferromagnetic correlations in the hubbard model with ultracold atoms, Nature (London) **519**, 211 (2015).

[31] L. Tarruell and L. Sanchez-Palencia, Quantum simulation of the hubbard model with ultracold fermions in optical lattices, Compt. Rend. Phys. **19**, 365 (2018).

[32] C. S. Chiu, G. Ji, A. Bohrdt, M. Xu, M. Knap, E. Demler, F. Grusdt, M. Greiner, and D. Greif, String patterns in the doped hubbard model, Science **365**, 251 (2019).

[33] J. Salfi, J. A. Mol, R. Rahman, G. Klimeck, M. Y. Simmons, L. C. L. Hollenberg, and S. Rogge, Quantum simulation of the hubbard model with dopant atoms in silicon, Nat. Commun. **7**, 11342 (2016).

[34] T. Esslinger, Fermi-hubbard physics with atoms in an optical lattice, Annu. Rev. Condens. Matter Phys. **1**, 129 (2010).

[35] T. A. Hilker, G. Salomon, F. Grusdt, A. Omran, M. Boll, E. Demler, I. Bloch, and C. Gross, Revealing hidden antiferromagnetic correlations in doped hubbard chains via string correlators, Science **357**, 484 (2017).

[36] E. Cocchi, L. A. Miller, J. H. Drewes, M. Koschorreck, D. Pertot, F. Brennecke, and M. Köhl, Equation of State of the Two-Dimensional Hubbard Model, Phys. Rev. Lett. **116**, 175301 (2016).

[37] S. Hirthe, T. Chalopin, D. Bourgund, P. Bojović, A. Bohrdt, E. Demler, F. Grusdt, I. Bloch, and T. A. Hilker, Magnetically mediated hole pairing in fermionic ladders of ultracold atoms, Nature **613**, 463 (2023).

[38] A. Bohrdt, L. Homeier, C. Reinmoser, E. Demler, and F. Grusdt, Exploration of doped quantum magnets with ultracold atoms, Annal. Phys. **435**, 168651 (2021).

[39] A. Wietek, Y. Y. He, S. R. White, A. Georges, and E. M. Stoudenmire, Stripes, Antiferromagnetism, and the Pseudogap in the Doped Hubbard Model at Finite Temperature, Phys. Rev. X **11**, 031007 (2021).

[40] B.-X. Zheng, C.-M. Chung, P. Corboz, G. Ehlers, M.-P. Qin, R. M. Noack, H. Shi, S. R. White, S. Zhang, and G. K.-L. Chan, Stripe order in the underdoped region of the two-dimensional hubbard model, Science **358**, 1155 (2017).

[41] A. Bohrdt, L. Homeier, I. Bloch, E. Demler, and F. Grusdt, Strong pairing in mixed-dimensional bilayer antiferromagnetic mott insulators, Nat. Phys. **18**, 651 (2022).

[42] F. Grusdt, Z. Zhu, T. Shi, and E. Demler, Meson formation in mixed-dimensional $t-J$ models, SciPost Phys. **5**, 057 (2018).

[43] L.-M. Duan, E. Demler, and M. D. Lukin, Controlling Spin Exchange Interactions of Ultracold Atoms in Optical Lattices, Phys. Rev. Lett. **91**, 090402 (2003).

[44] S. Trotzky, P. Cheinet, S. Fölling, M. Feld, U. Schnorrberger, A. M. Rey, A. Polkovnikov, E. A. Demler, M. D. Lukin, and I. Bloch, Time-resolved observation and control of superexchange interactions with ultracold atoms in optical lattices, Science **319**, 295 (2008).

[45] I. Dimitrova, N. Jepsen, A. Buyskikh, A. Venegas-Gomez, J. Amato-Grill, A. Daley, and W. Ketterle, Enhanced Superexchange in a Tilted Mott Insulator, Phys. Rev. Lett. **124**, 043204 (2020).

[46] See Supplemental Material at http://link.aps.org/supplemental/10.1103/PhysRevResearch.5.L022027 for details regarding the DMRG implementation and a discussion about tilted Fermi-Hubbard ladders.

[47] U. Schollwöck, The density-matrix renormalization group in the age of matrix product states, Annal. Phys. **326**, 96 (2011).

[48] U. Schollwöck, The density-matrix renormalization group, Rev. Mod. Phys. **77**, 259 (2005).

[49] S. R. White, Density Matrix Formulation for Quantum Renormalization Groups, Phys. Rev. Lett. **69**, 2863 (1992).

[50] C. Hubig, F. Lachenmaier, N.-O. Linden, T. Reinhard, L. Stenzel, A. Swoboda, M. Grundner, and S. Mardazad, The SyTen toolkit, https://syten.eu.

[51] C. Hubig, Symmetry-protected tensor networks, Dissertation, LMU Munich, Faculty of Physics (2017).

[52] H. J. Schulz, Correlation Exponents and the Metal-Insulator Transition in the One-Dimensional Hubbard Model, Phys. Rev. Lett. **64**, 2831 (1990).

[53] A. Nocera and G. Alvarez, Symmetry-conserving purification of quantum states within the density matrix renormalization group, Phys. Rev. B **93**, 045137 (2016).

[54] S. Paeckel, T. Köhler, A. Swoboda, S. R. Manmana, U. Schollwöck, and C. Hubig, Time-evolution methods for matrix-product states, Ann. Phys. **411**, 167998 (2019).

[55] A. E. Feiguin and G. A. Fiete, Spectral properties of a spin-incoherent luttinger liquid, Phys. Rev. B **81**, 075108 (2010).

[56] F. Grusdt and L. Pollet, $\mathbb{Z}_2$ Parton Phases in the Mixed-Dimensional $t-J_z$ Model, Phys. Rev. Lett. **125**, 256401 (2020).

[57] O. Zachar, S. A. Kivelson, and V. J. Emery, Landau theory of stripe phases in cuprates and nickelates, Phys. Rev. B **57**, 1422 (1998).

[58] A. Bohrdt, C. S. Chiu, G. Ji, M. Xu, D. Greif, M. Greiner, E. Demler, F. Grusdt, and M. Knap, Classifying snapshots of the doped hubbard model with machine learning, Nat. Phys. **15**, 921 (2019).

[59] A. J. Ferris and G. Vidal, Perfect sampling with unitary tensor networks, Phys. Rev. B **85**, 165146 (2012).

[60] M. Buser, U. Schollwöck, and F. Grusdt, Snapshot-based characterization of particle currents and the hall response in synthetic flux lattices, Phys. Rev. A **105**, 033303 (2022).

[61] Y.-R. Shu, M. Dupont, D.-X. Yao, S. Capponi, and A. W. Sandvik, Dynamical properties of the $s=\frac{1}{2}$ random heisenberg chain, Phys. Rev. B **97**, 104424 (2018).

[62] H. V. Kruis, I. P. McCulloch, Z. Nussinov, and J. Zaanen, Geometry and the hidden order of luttinger liquids: The universality of squeezed space, Phys. Rev. B **70**, 075109 (2004).

[63] We compare the magnetic mixD system in squeezed space with the Heisenberg model, given by the Hamiltonian $\hat{\mathcal{H}} = J\sum_{\langle \mathbf{i},\mathbf{j}\rangle} \hat{\mathbf{S}}_\mathbf{i}\cdot\hat{\mathbf{S}}_\mathbf{j}$, where J is the magnetic coupling constant and $\langle \mathbf{i},\mathbf{j}\rangle$ denotes nearest-neighbour pairs on a square lattice.

[64] H. Schlömer, T. Hilker, I. Bloch, U. Schollwöck, F. Grusdt, and A. Bohrdt, Quantifying hole-motion-induced frustration in doped antiferromagnets by Hamiltonian reconstruction, arXiv:2210.02440 (2022).